

# THE ORIGIN OF THE SPATIAL DISTRIBUTION OF X-RAY LUMINOUS AGN IN MASSIVE GALAXY CLUSTERS

JOSHUA T. RUDERMAN<sup>1</sup> AND HARALD EBELING

Institute for Astronomy, University of Hawaii, 2680 Woodlawn Drive, Honolulu, HI 96822

*ApJL, accepted*

## ABSTRACT

We study the spatial distribution of a 95% complete sample of 508 X-ray point sources (XPS) detected in the 0.5–2.0 keV band in Chandra ACIS-I observations of 51 massive galaxy clusters found in the MACS survey. Covering the redshift range  $z = 0.3 - 0.7$ , our cluster sample is statistically complete and comprises all MACS clusters with X-ray luminosities in excess of  $4.5 \times 10^{44}$  erg s<sup>-1</sup> (0.1–2.4 keV,  $h_0 = 0.7$ ,  $\Lambda$ CDM). Also studied are 20 control fields that do not contain clusters. We find the XPS surface density, computed in the cluster restframe, to exhibit a pronounced excess within 3.5 Mpc of the cluster centers. The excess, believed to be caused by AGN in the cluster, is significant at the  $8.0\sigma$  confidence level compared to the XPS density observed at the field edges. No significant central excess is found in the control fields. To investigate the physical origin of the AGN excess, we study the radial AGN density profile for a subset of 24 virialized clusters. We find a pronounced central spike ( $r < 0.5$  Mpc), followed by a depletion region at about 1.5 Mpc, and a broad secondary excess centered at approximately the virial radius of the host clusters ( $\approx 2.5$  Mpc). We present evidence that the central AGN excess reflects increased nuclear activity triggered by close encounters between infalling galaxies and the giant cD-type elliptical occupying the very cluster center. By contrast, the secondary excess at the cluster-field interface is likely due to black holes being fueled by galaxy mergers. In-depth spectroscopic and photometric follow-up observations of the optical counterparts of the XPS in a subset of our sample are being conducted to confirm this picture.

*Subject headings:* galaxies: active — galaxies: clusters: general — galaxies: evolution — galaxies: interactions — X-rays: galaxies — X-rays: galaxies: clusters

## 1. INTRODUCTION

The abundance and properties of AGN in galaxy clusters are important diagnostics for studies of cluster formation and galaxy evolution, but are difficult to measure as a large number of homogeneously selected systems is required for a statistically robust result. Massive galaxy clusters should be preferred targets for this kind of research as they constitute the largest reservoirs of galaxies. On the other hand, the galaxy population specifically of evolved clusters is overwhelmingly dominated by elliptical galaxies which, at least in the local universe, are gas-poor and thus do not typically exhibit nuclear activity. The situation is complicated further by the fact that, until recently, observational studies of the AGN distribution in clusters and the field have based AGN identifications almost exclusively on characteristic emission lines in the optical part of the galaxy spectrum, making them insensitive to a hypothetical population of extremely obscured AGN.

In the past few years, several studies have taken a complementary approach by using X-ray observations, specifically the surface density of X-ray point sources (XPS) around galaxy clusters, to quantify the AGN content of clusters relative to that of the field. Evidence of an XPS excess has been presented for several clusters over a wide range of redshifts and X-ray luminosities (Henry & Briel 1991; Cappi et al. 2001; Molnar et al. 2002; Sun & Murray 2002; Cappelluti et al. 2004). If the point sources detected in these fields are indeed at the cluster redshift, their X-ray luminosities suggest that the excess is caused by AGN in the cluster and can thus be used to map the cluster's AGN distribution. Optical follow-up observations performed in the field of A2104 at  $z = 0.154$  (Martini et al. 2002) confirm this picture

and reveal a possibly considerable fraction of these galaxies to lack the spectroscopic characteristics of AGN, suggesting that clusters may contain a large subset of optically obscured AGN.

Using Chandra ACIS-I data we here present the results of the first systematic study of the XPS content of a large, representative sample of massive galaxy clusters, to test the findings of earlier studies obtained for individual clusters. The large number of XPS detections obtained in this work allows us to construct the first resolved radial profile of XPS in the cluster rest frame, and to characterize the spatial XPS distribution as well as its likely physical origin. Throughout we assume a  $\Lambda$ CDM cosmology with  $h_0=0.7$ ,  $\Lambda=0.7$ , and  $\Omega=0.3$ .

## 2. FIELD SELECTION

We analyze Chandra ACIS data (front-illuminated chips only) for all 51 MACS clusters (MACS = Massive Cluster Survey) (Ebeling, Edge & Henry 2001) at  $z = 0.3 - 0.7$  that have been observed before Jan 15, 2005 and feature X-ray luminosities in excess of  $4.5 \times 10^{44}$  erg s<sup>-1</sup> (0.1–2.4 keV). The total geometric area covered by these observations is 5.73 deg<sup>2</sup>. An identical analysis is performed for ACIS-I data of 20 control fields, i.e. observations that did not target galaxy clusters, covering a total of 1.98 deg<sup>2</sup>. On-axis exposure times range from 10 ks to 87 ks. We reduce the raw data using CIAO software version 3.02, removing systematic instrumental effects and background flares. Merged datasets are created for the nine clusters observed twice and three clusters observed three times (see Fig. 1 for an example). To account for exposure-time variations across the ACIS field of view (vignetting, chip gaps, etc) we generate effective exposure maps for the observed XPS peak energy of 1.17 keV.

<sup>1</sup> also Departments of Physics and Mathematics, Stanford University, Stanford, CA 94305

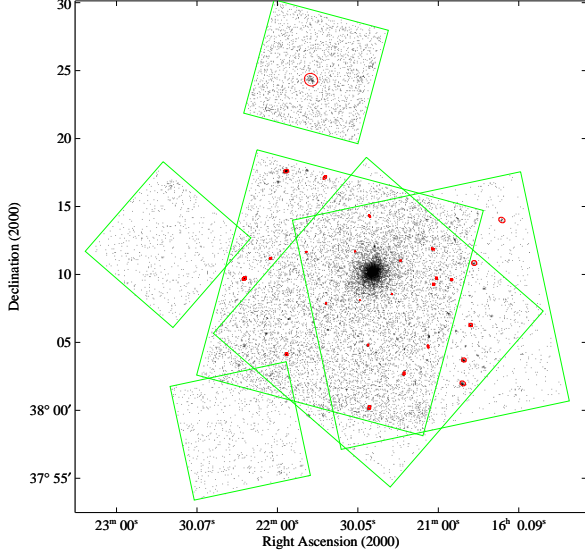


FIG. 1.— Merged dataset constructed from the three ACIS observations of the relaxed cluster MACSJ1621.3+3810 at  $z = 0.46$  (Edge et al. 2003). Red ellipses mark the point sources detected with *Celldetect* using a  $3\sigma$  detection threshold. The green rectangles show the orientation of the front-illuminated chips for the three individual exposures.

### 3. DATA REDUCTION

In order to maximize the detection efficiency we run the *Celldetect* algorithm in the 0.5–2.0 keV range<sup>2</sup>; only sources with detection significance of at least  $3\sigma$  above the local X-ray background are kept. For each cluster we use the appropriate ACIS exposure map to identify and remove spurious detections at the chip edges, leaving 910 point source detections in the cluster fields and 509 detections in the control fields.

Source count rates are converted to unabsorbed energy fluxes in the 0.5–2.0 keV energy band assuming the Galactic  $n_H$  value and a power law with a spectral index of  $\Gamma = 1.7$ , consistent with the observed stacked XPS spectrum<sup>3</sup>. Spatial variations of the detector characteristics are taken into account in the conversion by computing Redistribution Matrix Files (*RMF*) and Auxiliary Response Files (*ARF*) for each source individually. Using a power-law model of the XPS  $\log N - \log S$  obtained from a maximum-likelihood fit to the surface-density distribution of the XPS detected in 23 cluster observation of duration 17.5–20.5 ks, the most common exposure time, we compute instrumental flux limits of 95% completeness for each cluster scaled to individual exposure times. We find the source lists for all fields to be complete to a global flux limit of  $1.25 \times 10^{-14}$  erg s<sup>-1</sup> cm<sup>-2</sup>, corresponding to an on-axis exposure time of 10 ks. For point sources in cluster fields, we convert unabsorbed X-ray fluxes to luminosities assuming the point sources to be at the redshifts of the respective target cluster. Details of the properties of the target clusters as well as of the XPS population found in the corresponding ACIS-I fields will be presented in a forthcoming

<sup>2</sup> This bandpass is selected to maximize the signal-to-noise ratio for sources with AGN-like X-ray spectra

<sup>3</sup> The details of the chosen spectral model are not critical as, in this energy band, the observed flux depends only weakly on the chosen power law slope (Cappi et al. 2001).

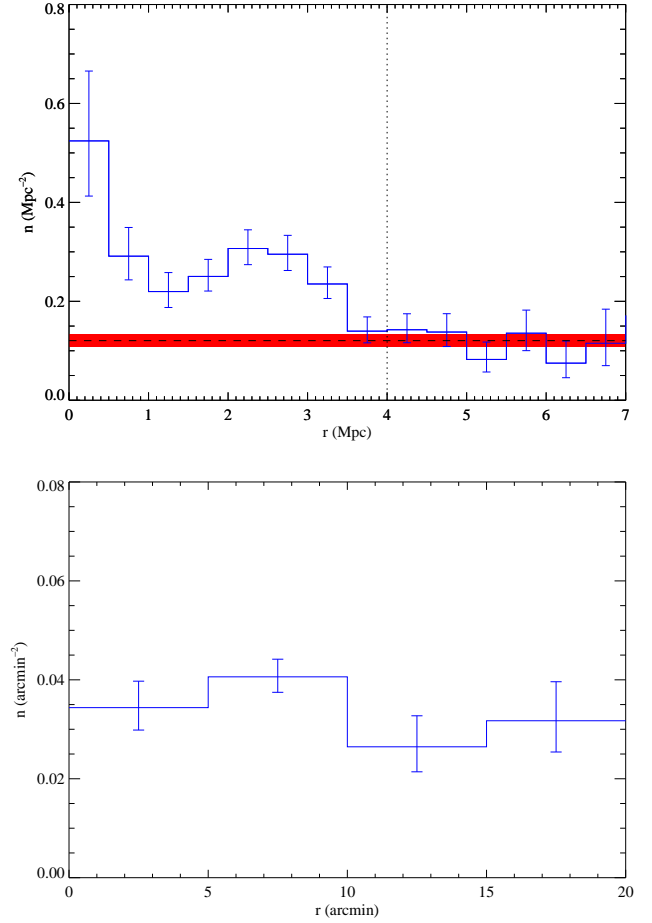


FIG. 2.— Radial profiles of the XPS surface density in 51 cluster fields (top) and 20 control fields (bottom). In the cluster fields, the XPS density is constant beyond distances of about 3.5 Mpc from the cluster center. The red bar marks this background level and its  $1\sigma$  error as derived from a fit to the data in the 4–7 Mpc region. Within 3.5 Mpc a highly significant ( $8.0\sigma$ ) excess is observed in the cluster fields. By contrast the XPS surface density in the control fields exhibits no excess. Both graphs probe similar angular scales because, at the redshifts of our clusters, one Mpc corresponds to 2.3 to 3.7 arcminutes.

paper (Ebeling et al., in preparation).

### 4. DISTRIBUTION OF POINT SOURCES

We compute the metric distance from the cluster center for all XPS detected in cluster fields, assuming again that the XPS are at the cluster redshift. A radial profile of their surface density is then constructed by binning the radial distances for the XPS from all 51 clusters, eliminating XPS fainter than the flux limit of the respective observation (this leaves 508 XPS), and dividing the XPS counts in each bin by the appropriate area. The result is shown in Fig. 2 (top). The graph at the bottom of the same figure shows a similar histogram for the 256 XPS detected above the individual flux limits of the 20 control fields, using the angular distances from the observation target position which corresponds to the location on the detector where cluster centers fall in cluster fields. For both panels of Fig. 2, as well as for Fig. 3, the value of the surface density in each bin is computed as  $n = \sum_i N_i / \sum_i A_i$ , with  $N_i$  and  $A_i$  being the XPS number and area of the respective annulus for the  $i^{\text{th}}$  cluster; the shown  $1\sigma$  error bars assume Poisson statistics using the analytic approximations of Ebeling (2003).

The significance of the central XPS excess observed in the cluster fields can be computed from the difference between the XPS surface density observed in the inner 3.5 Mpc of the cluster fields and the one observed in the outer 4–7 Mpc annulus, which we assume to be the background XPS density. We find the excess to be significant at the  $8.0\sigma$  confidence level. No central excess is observed in the radial XPS density profile for the control fields, ruling out a systematic instrumental effect or processing error. Note that the background per  $\text{Mpc}^2$  implied by the control fields is higher than the one measured in the outer regions of the cluster fields. We believe that this discrepancy reflects differences in the large-scale environment between the cluster and control samples which we will discuss in a future paper (Ebeling et al., in preparation).

### 5. CORRELATION WITH CLUSTER MORPHOLOGY

In order to gain insight into the physical origin of the radial XPS distribution shown in Fig. 2 (top) we crudely classify our 51 MACS clusters as relaxed or disturbed based on their X-ray morphology. Using Chandra images adaptively smoothed with the ASMOOTH algorithm (Ebeling White & Rangarajan 2005), we consider a cluster to be relaxed only if its X-ray surface-brightness distribution exhibits the following characteristics: a) on small scales, a pronounced central peak typical of a cooling core, and b) on large scales, near-perfect spherical symmetry. The combination of these criteria ensures that the clusters thus selected have not undergone a major merger event in several Gyr and can be considered virialized. For these systems the metric distance used to construct the histogram shown in Fig. 2 (top) corresponds to a well defined cluster-centric radius which probes values of the basic cluster properties — such as gas temperature and density, or galaxy velocity dispersion — that show little variation with azimuthal angle.

Our morphological classification splits our XPS list into two X-ray flux limited subsamples, each containing 254 XPS, detected in the fields of 24 relaxed or 27 disturbed systems, respectively. Fig. 3 shows the radial XPS density profiles for both subsets separately. Although both profiles exhibit a prominent excess of XPS within approximately 3.5 Mpc of the cluster center — significant at  $6.3$  and  $4.7\sigma$  confidence for relaxed and disturbed systems, respectively — the two distributions are markedly different (at  $3.0\sigma$  significance) with only the spherically symmetric, relaxed clusters showing the double peak apparent already in Fig. 2 (top).

### 6. CORRELATION WITH CLUSTER REDSHIFT

We attempt to also test how the excess depends on cluster redshift. In doing so, it is critical that the luminosities of the AGN probed at different redshifts are comparable, i.e., completeness to a universal *luminosity* limit needs to be ensured. For a first, crude check of any redshift dependence we divide our cluster sample into two subsets, comprising 29 clusters at  $z = 0.3 - 0.45$  and 21 clusters at  $z = 0.45 - 0.6$ . Converting the flux limits of the different observations into luminosities, we find that our XPS lists for the  $z = 0.3 - 0.6$  redshift range are 95% complete to a global luminosity limit of  $1.1 \times 10^{43} \text{ erg s}^{-1}$  (0.5–2.0 keV). Applying this luminosity cut reduces our XPS sample to 87 and 119 sources in the  $z = 0.3 - 0.45$  and  $z = 0.45 - 0.6$  cluster fields, respectively. Although the data are suggestive of an increase of the excess with redshift,

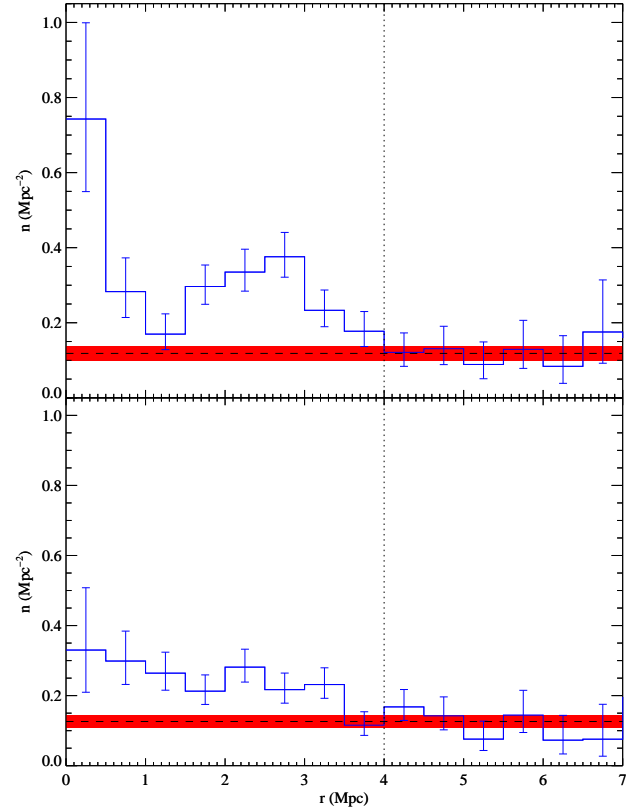


FIG. 3.— Radial profiles of the XPS surface density in the fields of 24 relaxed clusters (top) and in the fields of 27 disturbed clusters (bottom). The profile for relaxed clusters features a pronounced central peak at  $r < 0.5$  Mpc, a depletion region at 0.5–1.5 Mpc, and a broad secondary excess at approximately the virial radius of 2–3 Mpc. By contrast, the XPS density profile for disturbed clusters shows a smoothly distributed excess.

the difference between the two radial profiles is not significant ( $1.5\sigma$ ) at the current sizes of our subsamples.

## 7. DISCUSSION

### 7.1. XPS nature

The X-ray luminosities referred to in the previous section can be used to characterize the nature of the point sources causing the observed excess. As a result of the, in general, moderate exposure times of the ACIS observations used in our study, we find all of the XPS in our flux-complete sample to feature X-ray luminosities well in excess of  $3 \times 10^{42} \text{ erg s}^{-1}$  (0.5–8.0 keV). Since this value represents a tight upper limit to the X-ray luminosity of starburst galaxies (Bauer et al. 2004) we conclude that the observed XPS excess can be attributed to AGN at the cluster redshift.

The alternative explanation that the excess is caused by gravitational lensing of background AGN (which would then have to be yet more X-ray luminous) can be ruled out because of the large area over which the excess is observed. The amplification provided by lensing can account at best for a small fraction of the observed excess at  $r < 0.5$  Mpc, and is entirely negligible at the angular distances corresponding to the radius at which the secondary excess is observed (Smith et al. 2002). In addition, studies searching for an XPS excess in cluster fields observed to much lower X-ray fluxes indicate that the faint end of the  $\log N - \log S$  distribution of the excess is inconsistent with the one predicted for gravitationally

lensed sources (Cappi et al. 2001). We therefore conclude that the excess is due to AGN in the cluster.

### 7.2. XPS distribution

We now discuss the possible origin of the spatial XPS distribution, which is characterized by a central excess within 0.5 Mpc of the cluster core, a depletion region around 1.5 Mpc, and a broad secondary excess observed at about the virial radius of the relaxed clusters. Although present in the fields of all clusters, the excess at  $r < 0.5$  Mpc is much more pronounced for the relaxed systems, all of which possess central cooling cores dominated by massive cD galaxies. Closer inspection of the XPS distribution reveals that the difference in this first radial bin between relaxed and disturbed systems originates at yet smaller cluster-centric distances. We detect six XPS within 250 kpc of the cD galaxies in virialized clusters and none within the same distance of the cores of disturbed systems. Two of these six XPS in the very heart of virialized clusters can be unambiguously identified as AGN in the cD itself; for the other four cases we propose that the observed X-ray emission is due to nuclear activity triggered by close encounters between infalling cluster galaxies and the cD. Extending this picture to the remainder of the  $r < 0.5$  Mpc bin, we predict that the central excess is due to galaxy mergers and tidal interactions involving the giant elliptical galaxies dominating the centers of MACS clusters.

The AGN depletion zone in relaxed clusters at radii around 1.5 Mpc and the following broad excess at roughly the virial radius can be explained by a slightly different mechanism. The rise of the observed XPS surface density at 2 – 3 Mpc suggests increased AGN activity at the cluster-field interface, which is easily explained by merger-induced accretion onto massive black holes, favoured by the increase in galaxy density compared to the field and the presence of relatively gas-rich galaxies in this transition region. Since successful mergers require low collision velocities of typically less than 300 km s<sup>-1</sup> (Binney & Tremaine 1987) such mergers become extremely rare closer to the cluster core where, for MACS clusters, the galaxy velocity dispersion reaches and exceeds 1000 km s<sup>-1</sup> (Barrett et al., in preparation). As a result, the AGN density is dramatically reduced at intermediate radii (0.5–2 Mpc). In addition, activity triggered at larger radii will cease as infalling galaxies approach the cluster core since the timescale for the depletion of the accretion disk is substantially shorter than the cluster crossing time. The combination of these two effects ensures that the excess is confined to the infall region where AGN activity is triggered.

We expect the same physical mechanisms to cause AGN activity in disturbed clusters. However, since disturbed clusters lack well defined cores as well as spherical symmetry, the excess is spread much more evenly over the 0 – 3.5 Mpc range, as observed (Fig. 3, bottom).

### 8. CONCLUSIONS

We present results of the first study of the X-ray point source content of a statistically well defined sample of galaxy clusters, using Chandra/ACIS observations of 51 MACS clusters at  $z = 0.3 - 0.7$ . We detect an overall  $8.0\sigma$  significant excess in the point source density within 3.5 Mpc of cluster centers, which we argue is caused by AGN in the cluster targets of these observations. We also present the first resolved radial profile of the excess and find it to depend significantly on cluster morphology. Making use of the simple geometry afforded by relaxed clusters we are able to identify two distinct components to the excess, namely a central excess of AGN which we believe to be due to galaxy interactions involving the giant ellipticals near the cluster core, and a broad secondary excess at about the virial radius. We propose that the AGN activity causing the secondary excess is triggered by galaxy mergers, which are most likely to occur in the low-energy collisions favoured in the cluster-field transition region. The lack of AGN at intermediate radii can be explained by the low merger probability at high relative velocities and the shortness of the accretion timescale compared to the cluster crossing time.

Our results confirm those of past studies which have detected point source excesses in cluster fields and provide a novel way to probe the dynamics of AGN production by galaxy interactions in massive clusters. Future work will focus on the optical counterparts of X-ray point sources in selected MACS clusters to unambiguously identify redshifts and X-ray emission processes, thus testing conclusively our hypothesis that the excess is due to AGN cluster members.

The authors gratefully acknowledge financial support from NASA grant NAG 5-8253 and SAO grant GO2-3168X (HE), and from the National Science Foundation's Research Experiences for Undergraduates program (JTR). We thank everybody at the Chandra X-Ray Center for their contribution to a spectacularly successful satellite mission and specifically for maintaining the CIAO software package. Thanks also to Joshua Barnes for a very informative discussion about the physics and consequences of galaxy mergers, and to the referee, Stefano Ettori, for helpful comments and criticism.

### REFERENCES

- Bauer, F.E., Alexander, D.M., Brandt, W.N., Schneider, D.P., Treister, E., Hornschemeier, A.E., & Garmire, G.P. 2004, *ApJ*, 128, 2048  
 Binney, J. & Tremaine S. 1987, *Galactic Dynamics*, Princeton: Princeton University Press  
 Cappelluti, N., Cappi, M., Dadina, M., Malaguti, G., Branchesi, M., Delia, V., & Palumbo, G.G.C. 2004, *A&A*, in press  
 Cappi, M. et al. 2001, *ApJ*, 548, 624  
 Ebeling, H., Edge, A.C., & Henry, J.P. 2001, *ApJ*, 553, 668  
 Ebeling, H. 2003, *MNRAS*, 340, 1269  
 Ebeling, H., White, D.A., & Rangarajan V.N. 2005, *MNRAS*, submitted  
 Edge, A.C., Ebeling, H., Bremer, M., Röttgering, H., van Haarlem, M.P., Rengelink, R., Courtney, N.J.D. 2003, *MNRAS*, 339, 913  
 Henry, J.P., & Briel, U.G. 1991, *A&A*, 246, 14L  
 Martini, P., Kelson, D.D., Mulchaey, J.S. & Trager, S.C. 2002, *ApJ*, 576, L109  
 Molnar, M.S., Hughes, J.P., Donahue, M. & Joy, M. 2002, *ApJ*, 573, L91  
 Smith, G.P. et al. 2002, *MNRAS*, 330, 1  
 Sun, M., & Murray, S.S. 2002, *ApJ*, 577, 139